Supplementary material: Dependence of the self-diffusion coefficient on the q-gap value in fluids

Konstantin P. Zhukov, Nikita P. Kryuchkov,* and Stanislav O. Yurchenko
Bauman Moscow State Technical University, 2nd Baumanskaya Street 5, 105005 Moscow, Russia
(Dated: December 16, 2025)

MOLECULAR DYNAMICS SIMULATIONS DETAILS

We considered systems of particles interacting via the Lennard-Jones (LJ) and Yukawa (Ykw) pair potentials:

$$\varphi_{\mathrm{LJ}}(r) = 4\varepsilon\left[\left(\frac{\sigma}{r}\right)^{12} - \left(\frac{\sigma}{r}\right)^{6}\right], \tag{1}$$

$$\varphi_{\mathrm{Ykw}}(r) = A\frac{e^{-k_D r}}{r}, \tag{2}$$

where ε and σ are the energy and length scale of the interaction, respectively; A and k_D are parameters which where chosen as $A = 1$, $k_D = \lambda_D^{-1} = 1$. Corresponding coupling and screening parameters are $\Gamma = A(ak_BT)^{-1}$ and $\kappa = a\lambda_D^{-1}$, respectively. Here λ_D is the Debye length, $a = (3/4\pi n)^{1/3}$ is the Wigner-Seitz radius, where $n = N/V$ is the numerical density, k_B is the Boltzmann constant and T is the temperature.

We have studied 3D and 2D fluids consisting of $N = 4000$ ($N = 4900$ in 2D case) particles in an NVT ensemble with a Nose–Hoover thermostat. The initial state of the system was a cubic lattice (a square in 2D case) with a size $L = 10$ ($L = 70$ in 2D case) with periodic boundary conditions with Maxwell distribution of velocities. The cutoff radius of interaction was chosen as $r_{\mathrm{cut}} = 7.5n^{-1/d}$, where $n = N/V$ is the numerical density and d is the space dimension. The mass m, length σ, and energy ε were normalized to unity.

The interatomic potential with machine learning (ML-IAP) for liquid aluminum [1] was also considered:

$$\varphi_{\text{ML-IAP}}(r) = \varphi_{\mathrm{ref}}(r) + \sum_{i=1}^{N} E^i_{\mathrm{SNAP}}, \tag{3}$$

where E_{ref} denotes a reference potential and E^i_{SNAP} is the total energy of atom i relative to the atoms in its neighborhood, governed by the spectral neighbor analysis potential method (SNAP) [2]. Ziegler-Biersack-Littmark (ZBL) potential [3] is used as a reference potential. The SNAP energy for each atom is calculated using a linear combination of the bispectrum components $\mathbf{B}^i$

$$E^i_{\mathrm{SNAP}} = \boldsymbol{\beta} \times \mathbf{B}^i, \tag{4}$$

where $\boldsymbol{\beta}$ are linear coefficients and $\mathbf{B}^i$ are descriptors of the local environment of atom i. Obtained using machine learning coefficients [4] $\boldsymbol{\beta}$ were used in this work.

Table I. Chosen states of considered systems.

Potential	Dimension	Density	Temperature
ML-IAP (Al)	3D	2.7 g/cm^3	1560 — 2560 K
EAM (Fe)	3D	3.6 g/cm^3	1812 — 2392 K
LJ	3D	1.00	1.6 — 7.0
		1.10	2.7 — 8.0
		1.20	4.0 — 9.0
		1.30	5.8 — 15.6
		1.40	8.1 — 17.9
		1.60	14.6 — 21.8
		1.80	24.2 — 29.8
		2.00	37.4 – 44.8
	2D	0.80	0.60 — 3.10
		0.85	1.00 — 3.50
		0.90	2.00 — 4.50
Yukawa		κ	Γ
	3D	1.00	217 — 117
		1.25	250 — 110
		1.50	270 — 86
		2.00	440 — 157
		2.50	750 — 305
		3.00	1185 — 665
	2D	1.00	177 — 77
		1.50	250 — 73
		2.00	395 — 112

Simulations of liquid Al were performed in a three-dimensional face-centered cubic box with dimensions of $Lx = Ly = Lz = 10a$, where a is lattice constant, with mass density $\rho = 2.7\mathrm{g/cm}^3$. The remaining simulation details including number of particles, thermostating and boundary conditions follow previously established setup.

Moreover, we considered liquid iron using Embedded atom model (EAM). The general form of this potential can be expressed as:

$$E_i = \sum_i F(\rho_i) + \frac{1}{2}\sum_i \sum_{j\neq i} \varphi_{\mathrm{p}}(r_{ij}), \tag{5}$$

where $F_i(\rho_i)$ denotes the embedding energy for atom i, a function of the local electron density ρ_i. This local density is computed as a superposition of the contributions from all neighboring atoms j:

$$\rho_i = \sum_{j\neq i} \rho(r_{ij}). \tag{6}$$

In these expressions, $\varphi_{\rm p}(r_{ij})$ represents the pairwise potential between atoms i and j, separated by a distance r_{ij}. The specific functional forms for $F(\rho)$, $\rho(r)$, and $\varphi_{\rm p}(r)$ employed in this work are those established in the corresponding paper [5].

The mass density $\rho = 10g/cm^3$ was used in the simulations for liquid iron. The remaining simulation parameters correspond to those employed for liquid iron.

Simulations of fluids of particles interacting via the Lennard-Jones and Yukawa potentials were performed using the numerical time step $\Delta t = 5 \times 10^{-3}\sqrt{m\sigma^2/\varepsilon}$. For ML-IAP and EAM potentials in liquid aluminum and iron the time step $\Delta t = 5$ fs was chosen. All simulations where performed with the LAMMPS package [6] for 5×10^4 time steps, where the first 5000 were used for system relaxation.

Table I shows the parameters of examined systems states.

RESULTS

Figure 1 presents the example of computed velocity current spectra for 3D Lennard-Jones fluid with density $n = 1$ at temperatures **(a–c)** 2 and **(d–f)** 6. Data where estimated using two-oscillator model (Eq. 3 in main article). Corresponding fits are represented with solid line on the plots.

By obtaining the mode frequencies from the approximation we analyzed dispersion relations $\omega_{L,T}(q)$ to calculate q-gap values. Figure 2 represents dispersion relation for Lennard-Jones fluid at $n = 1$, $T = 5$. The longitudinal and transverse modes (circles) with linear approximations (solid lines) are shown in gray and orange colors, respectively. Red node q_g indicates the q-gap region in low-frequency branch $\omega_T(q)$. The dark gray zone corresponds to the region of $qn^{-1/3} < 2\pi/L$.

To calculate self-diffusion coefficient D we used mean-squared displacement (MSD) of particles. The MSD(t) dependencies for Lennard-Jones fluid are illustrated in Figure 3 for both **(a)** 3D and **(b)** 2D cases at temperatures 2 and 1.2 respectively.

The dependencies of self-diffusion coefficient (SDC) on q-gap width for liquid Al and Fe are presented on Figure 4 in red and blue colors respectively. Solid lines represent linear approximations, consistent with the results reported for other systems in the main article.

We compared the results for the Lennard–Jones and Yukawa fluids with those obtained for extended systems in the same states. The simulation box was enlarged such that $L_{\rm ext} = 1.5L_{\rm orig}$. The resulting dependencies closely match those of the original systems, as illustrated in Fig. 5. Data for the original systems are shown in red, and those for the extended systems in blue, along with their respective linear fits.

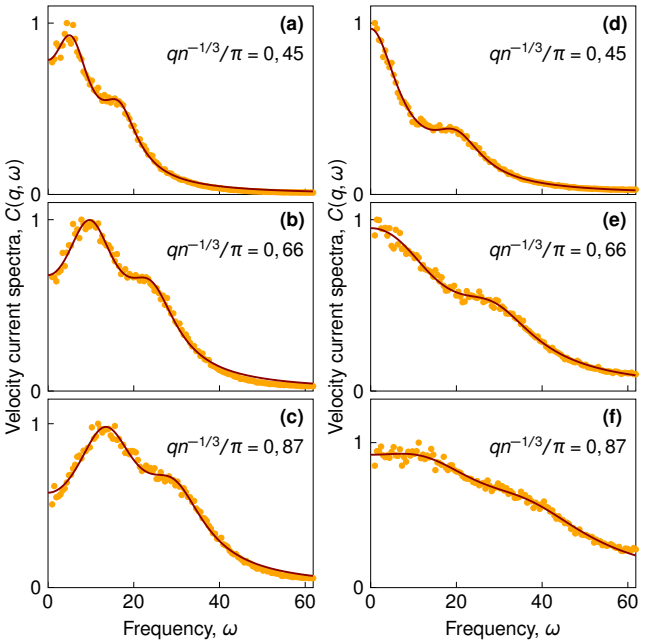

Figure 1. Transverse modes of dispersion relations for a three-dimensional fluids with the Lennard-Jones potential. Panels **(a–c)** show spectra for a system with density $n = 1$ at $T = 2$, obtained from velocity flux power spectra analysis using two-oscillator model. For panels **(d–f)**, results are obtained at $n = 1$ and $T = 6$, with the same description as for panels (a–c).

Obtained q-gap values near the melting point (MP) – $q_{g,\rm MP}$ are presented in Table II along with the slopes of $D(q_g)$ dependencies for each considered system.

In main article we observed universal relationship between the self-diffusion coefficient value in MP $D_{\rm MP}$ and the slope of $D(q_g)$ dependence $\dot{D}$ which can be described by fit 7

$$D_{\rm MP} \approx \left(\frac{{\rm d}D}{{\rm d}q_g}\right)^2 + C_{\rm MP}, \tag{7}$$

where $C_{\rm MP} = 9.2 \cdot 10^{-4}$. Using this equation we reconstructed initial $D(q_g)$ dependencies in form:

$$D = D_{\rm MP} + \mathfrak{D}(q_g - q_{g,\rm MP}), \tag{8}$$

where $\mathfrak{D} = \sqrt{D_{\rm MP} - C_{\rm MP}}$. The comparison between obtained phenomenological form and initial data for 3D LJ, Yukawa and Al systems is presented in Figure 6

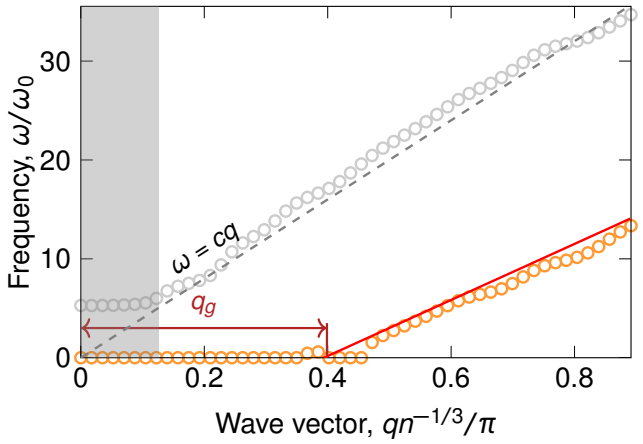

Figure 2. Dispersion relations $\omega_{L,T}(q)$ for a 3D Lennard-Jones fluid at density $n = 1$ and temperature $T = 5$. Transverse (ω_T) and longitudinal (ω_L) modes are represented by orange and gray circles, respectively. The gray and red lines depict the theoretical asymptotic curves $\omega = cq$. The dark gray zone indicates the region where $qn^{-1/3} < 2\pi/L$ and finite-size effects are significant (L being the system size).

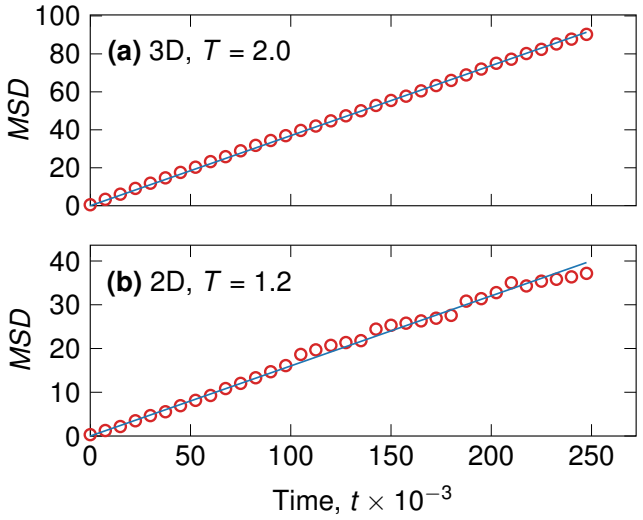

Figure 3. Dependence of the MSD on the time t for the Lennard-Jones potential in three- and two-dimensional cases.

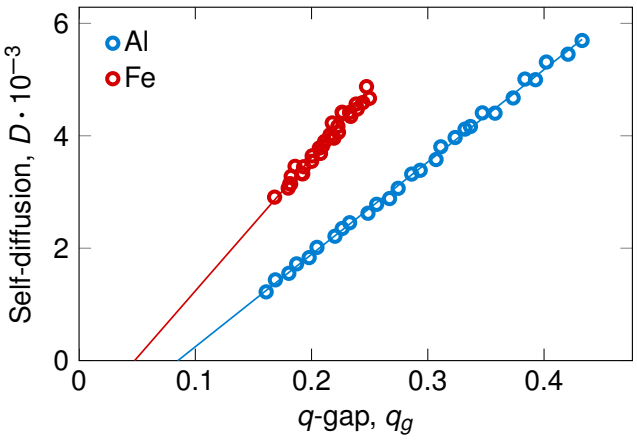

Figure 4. Dependence of the self-diffusion coefficient D on the q-gap width for 3D liquid aluminum (red) at and iron (blue).

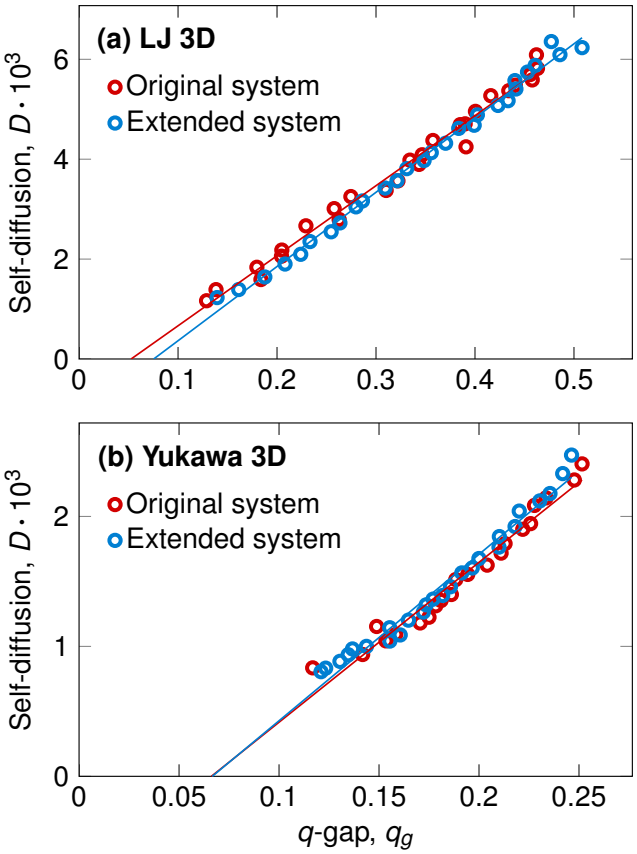

Figure 5. The comparison between $D(q_g)$ relations in extended (blue) and original (red) 3D systems with Lennard-Jones ($n = 1$) and Yukawa ($\kappa = 1$) potentials.

Table II. Minimum values of q_g and corresponding slopes for studied systems

Potential	Dimension	Density	Value of q_g near the MP, $q_{g,\mathrm{MP}}$	$\left(\frac{\mathrm{d}D}{\mathrm{d}q_g}\right)$
ML-IAP (Al)	3D	2.7 g/cm^3	0.078	0.013
EAM (Fe)	3D	3.6 g/cm^3	0.168	0.024
LJ	3D	1.0	0.165	0.0166
		1.1	0.159	0.0142
		1.2	0.157	0.0136
		1.3	0.151	0.0124
		1.4	0.151	0.0110
		1.6	0.169	0.0079
		1.8	0.182	0.0074
		2.0	0.170	0.0062
	2D	0.80	0.172	
		0.85	0.119	
		0.90	0.056	
		κ		
Yukawa	3D	1.00	0.115	0.015
		1.25	0.105	0.027
		1.50	0.123	0.042
		2.00	0.106	0.052
		2.50	0.130	0.058
		3.00	0.111	0.098
	2D	1.00	0.090	
		1.50	0.097	
		2.00	0.129	

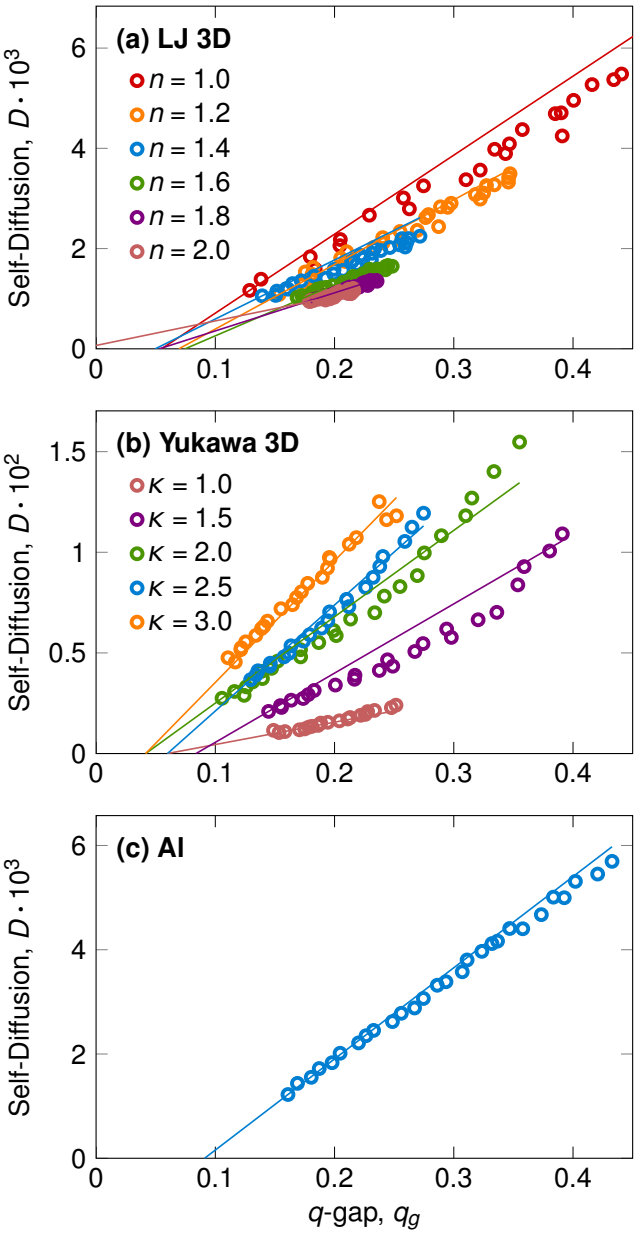

Figure 6. The comparison between obtained phenomenological form (solid lines) and initial data (circles) for 3D **(a)** LJ, **(b)** Yukawa and **(c)** Al.

* kruchkov_nkt@mail.ru

[1] S. Kumar, H. Tahmasbi, K. Ramakrishna, M. Lokamani, S. Nikolov, J. Tranchida, M. A. Wood, and A. Cangi, Transferable interatomic potential for aluminum from ambient conditions to warm dense matter, Physical Review Research **5**, 033162 (2023).

[2] A. Thompson, L. Swiler, C. Trott, S. Foiles, and G. Tucker, Spectral neighbor analysis method for automated generation of quantum-accurate interatomic potentials, Journal of Computational Physics **285**, 316 (2015).

[3] The Stopping and Range of Ions in Matter, in *Treatise on Heavy-Ion Science* (Springer US, Boston, MA, 1985) pp. 93–129.

[4] S. Kumar, H. Tahmasbi, K. Ramakrishna, M. Lokamani, S. Nikolov, J. Tranchida, M. A. Wood, and A. Cangi, Training scripts and input data sets: Transferable Interatomic Potential for Aluminum from Ambient Conditions to Warm Dense Matter (2023).

[5] A. B. Belonoshko, R. Ahuja, and B. Johansson, Quasi– *Ab Initio* Molecular Dynamic Study of Fe Melting, Physical Review Letters **84**, 3638 (2000).

[6] S. Plimpton, Fast Parallel Algorithms for Short-Range Molecular Dynamics, Journal of Computational Physics **117**, 1 (1995).